--Supporting Information--

Dry Pressing Neat Active Materials into Ultrahigh Mass Loading Sandwich Cathodes Enabled by Holey Graphene Scaffold

Christian O. Plaza-Rivera, Brandon A. Walker, Nam X. Tran, Rocco P. Viggiano, Donald A. Dornbusch, James J. Wu, John W. Connell, and Yi Lin**

Email: yi.lin-1@nasa.gov; john.w.connell@nasa.gov

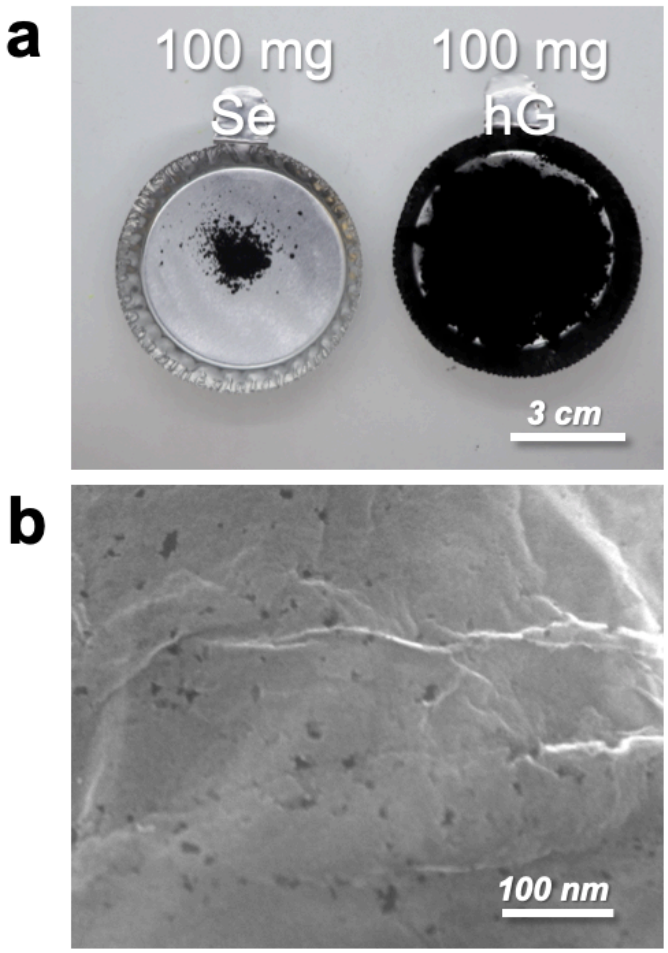

Figure S1. (a) Photograph of 100 mg Se powder and 100 mg hG powder. (b) A typical SEM image of a hG sheet.

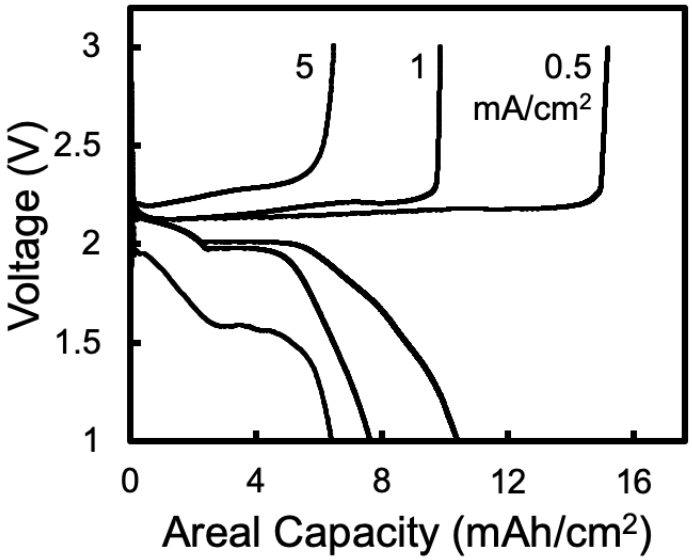

Figure S2. Areal capacity performances from the first discharge and the first charge of three identical Li-Se batteries (m_{Se} = 17.3 mg/cm^2, Se% ~ 75 wt%) ran at 0.5, 1, and 5 mA/cm^2, respectively, in the voltage window of 1 – 3 V. This is the same set of data shown in Figure 2c but only with the x-axis converted into areal capacity.

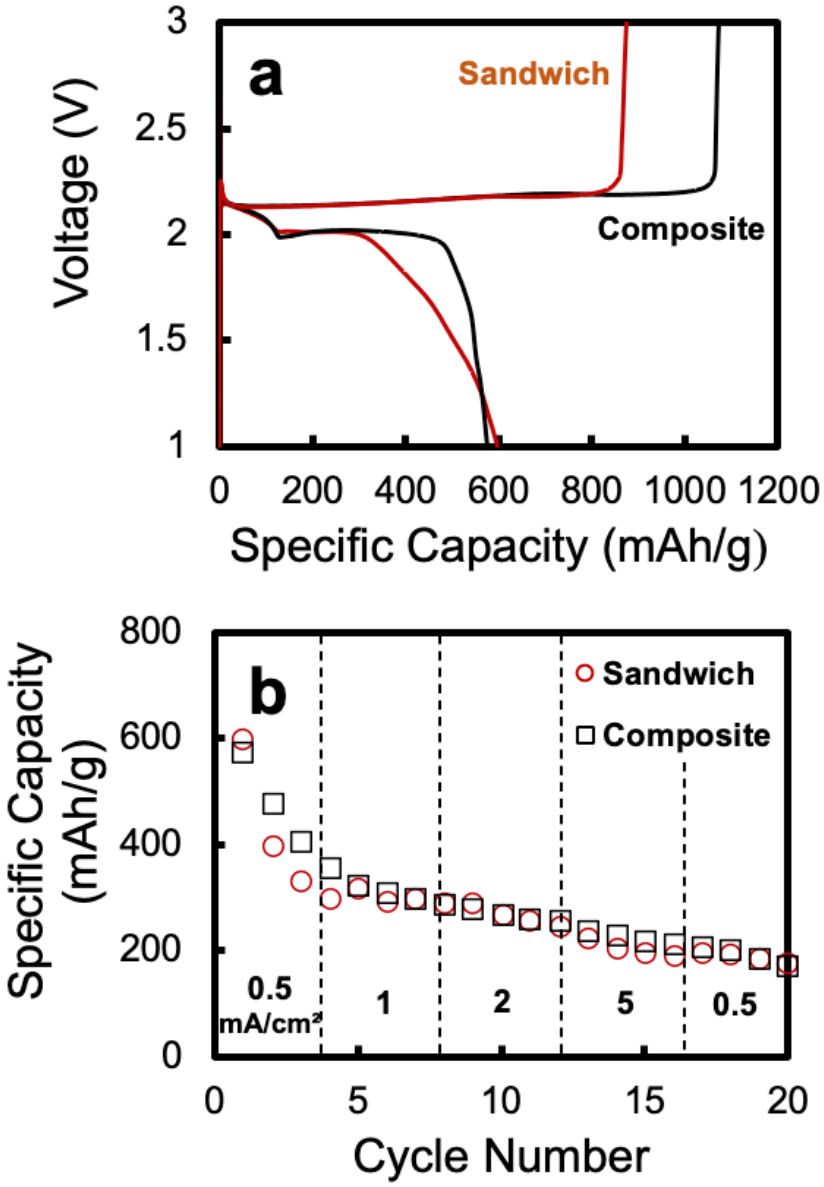

Figure S3. Performance comparison of Li-Se batteries with a hG/Se/hG sandwich cathode vs a hG/Se composite cathode where hG and Se powders were pre-mixed: (a) the first discharge and the first charge curves; (b) specific capacity change at different current densities of 0.5, 1, 2, 5, and 0.5 mA/cm^2. The total mass of the active material layer were kept the same (30 mg), so that their Se mass loadings and Se contents were slightly different (sandwich: m_{Se} = 17.3 mg/cm^2, Se% ~ 75 wt%; composite: m_{Se} = 15.6 mg/cm^2, Se% ~ 90 wt%).

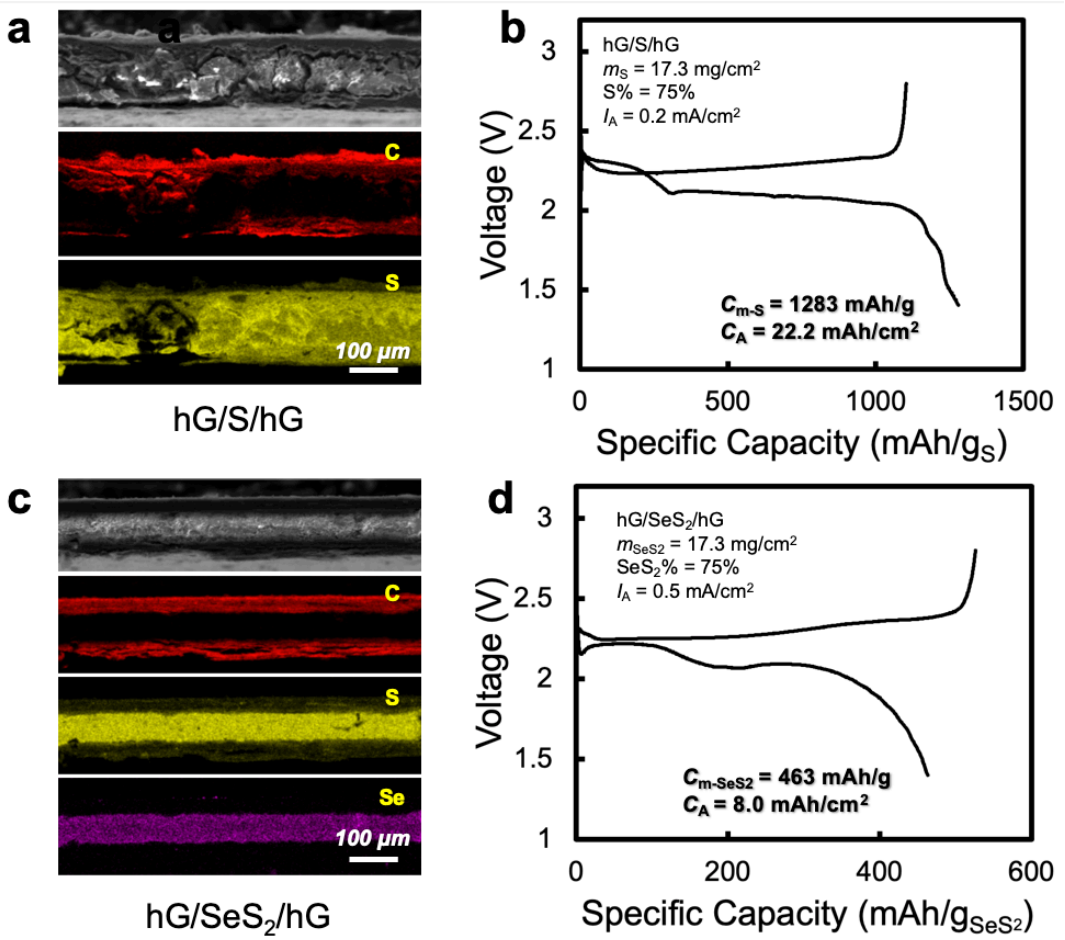

Figure S4. hG-enabled sandwich electrodes with (a,b) S and (c,d) SeS_2 as the active material, respectively. (a,c) are the SEM and the corresponding elemental maps of the electrode cross-section. (b,d) are the first discharge and the first charge curves of batteries made with the corresponding sandwich electrode. The electrode characteristics and measurement parameters are specified on each plot. m_S: S mass loading; m_{SeS2}: SeS_2 mass loading; $C_{m\text{-}S}$ and $C_{m\text{-}SeS2}$: specific capacity based on the weight of S and SeS_2, respectively; C_A: areal capacity; I_A: areal current density.

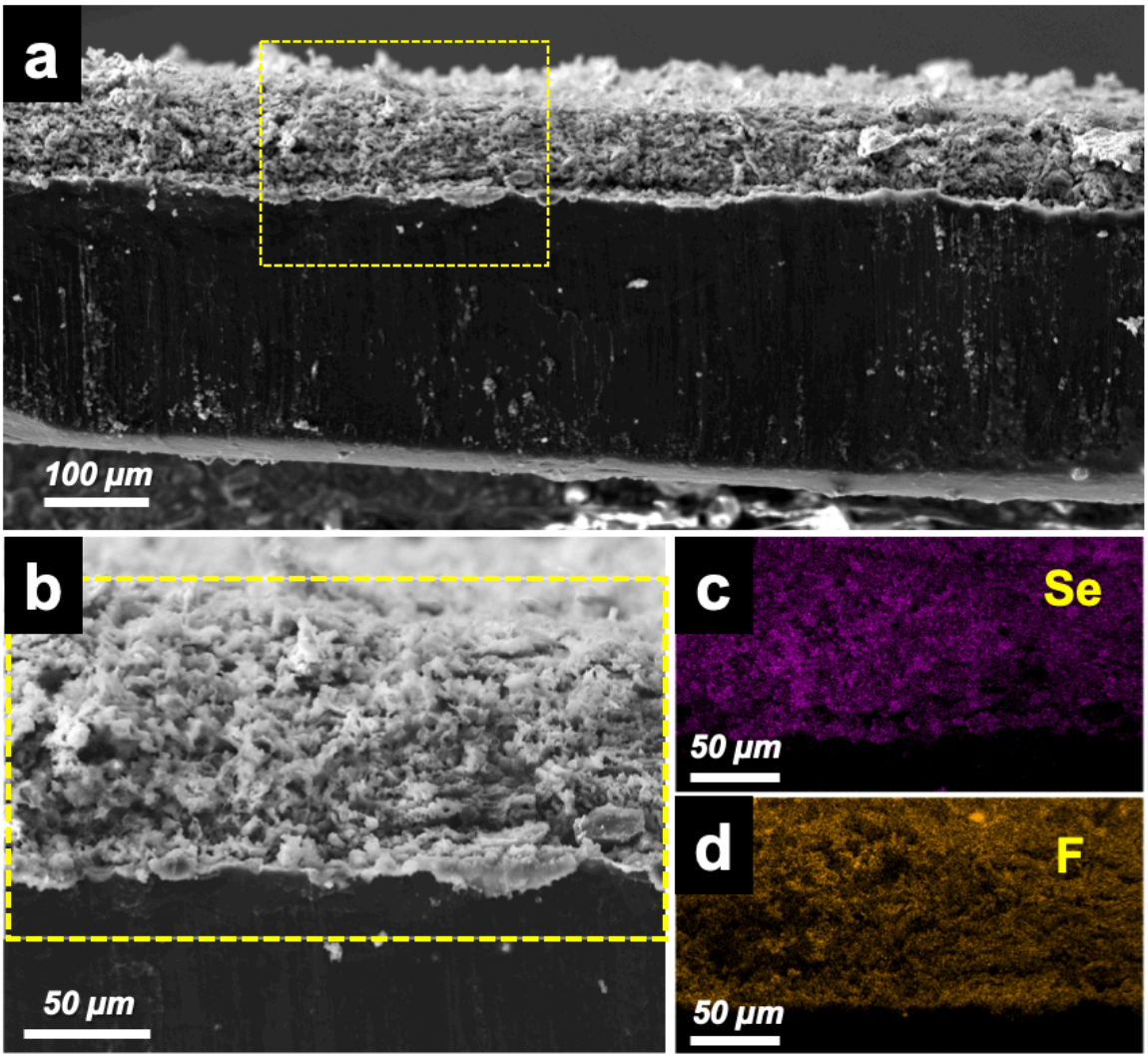

Figure S5. (a) A typical SEM image of cross-section of the Li anode of the Li-Se battery with the hG/Se/hG sandwich cathode (m_{Se} = 17.3 mg/cm^2, Se% ~ 75 wt%) after the first discharge (1 D). (b) A magnified view from the area highlighted in (a). (c) Se and (d) F map from EDS analyses of the area highlighted in (b). F element is an indication of SEI as it originated from the electrolyte (LiTFSI).

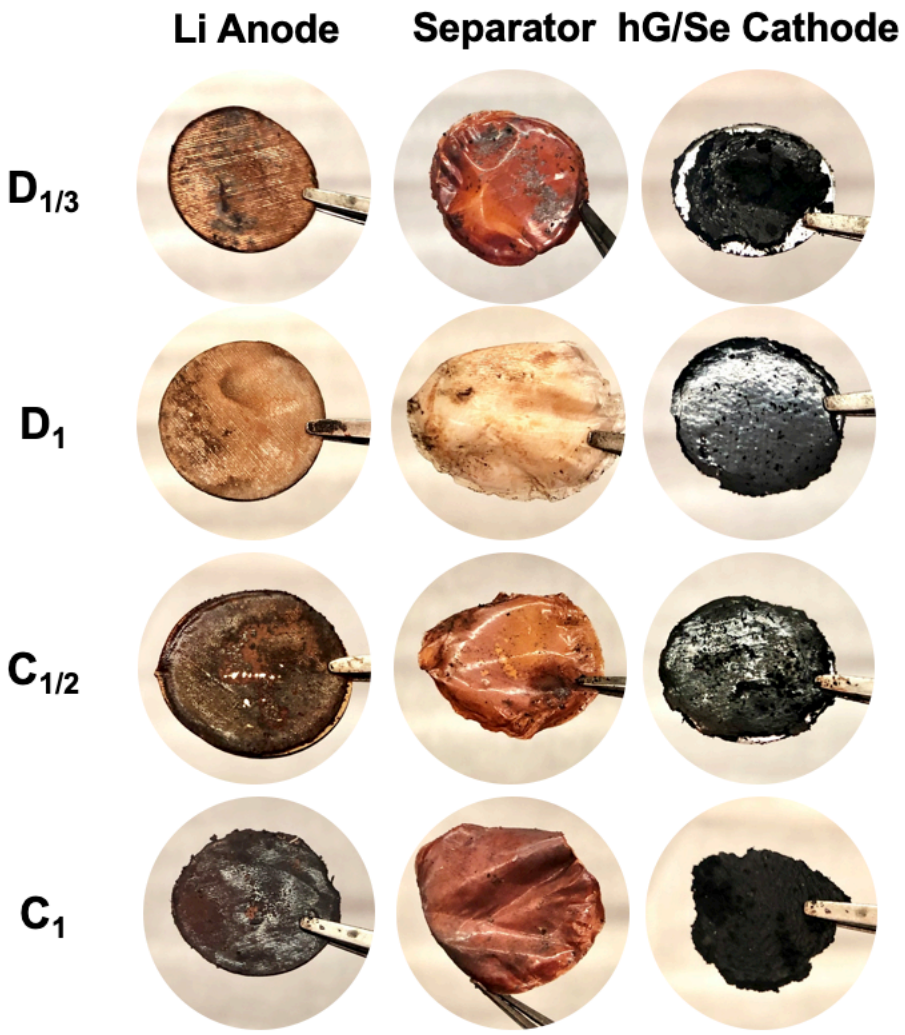

Figure S6. Photographs of post-mortem Li anodes, separators, and the hG/Se cathodes of identical Li-Se batteries with the hG/Se/hG sandwich cathode (m_{Se} = 17.3 mg/cm^2, Se% ~ 75 wt%) that were discharged or charged to different extents at 1 mA/cm^2.

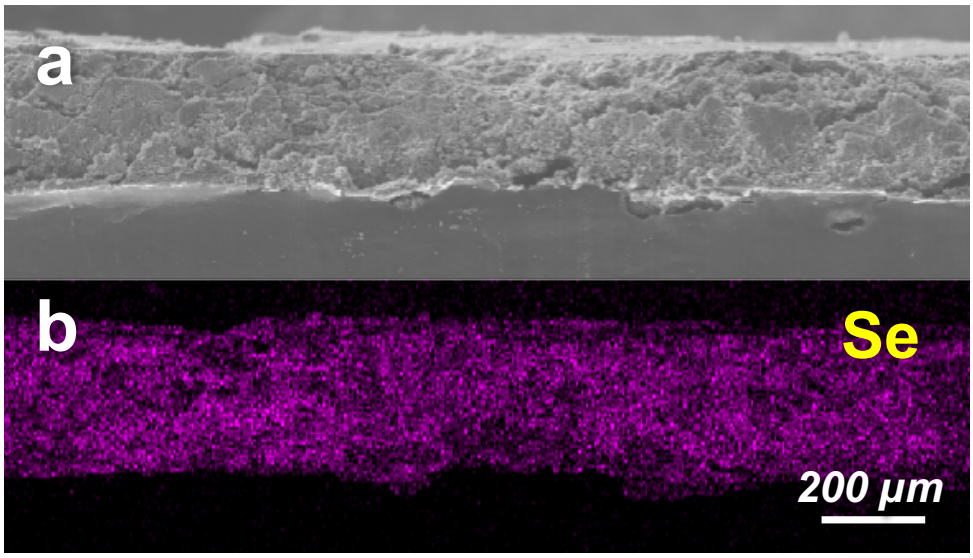

Figure S7. (a) Post-mortem SEM image and (b) the corresponding Se map from EDS mapping of the cathode cross-section, originally in hG/Se/hG sandwich architecture (m_{Se} = 17.3 mg/cm^2, Se% ~ 75 wt%), from a Li-Se batteries that were run for > 200 cycles at 1 mA/cm^2.

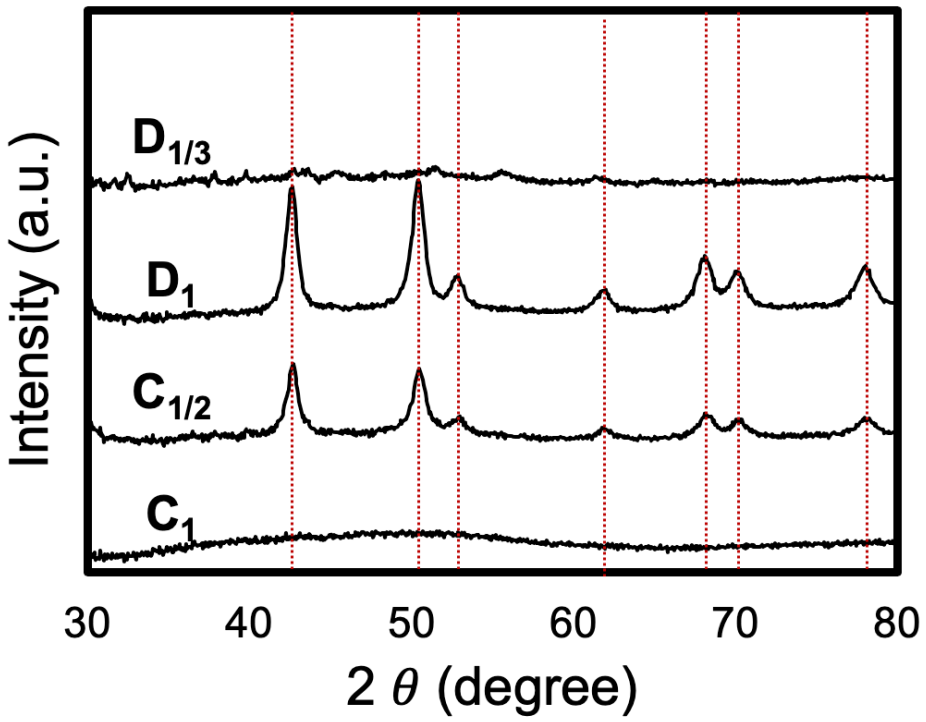

Figure S8. Post-mortem XRD patterns of various cathodes, originally in hG/Se/hG sandwich architecture (m_{Se} = 17.3 mg/cm^2, Se% ~ 75 wt%), from identical Li-Se batteries that were discharged or charged to different extents at 1 mA/cm^2.

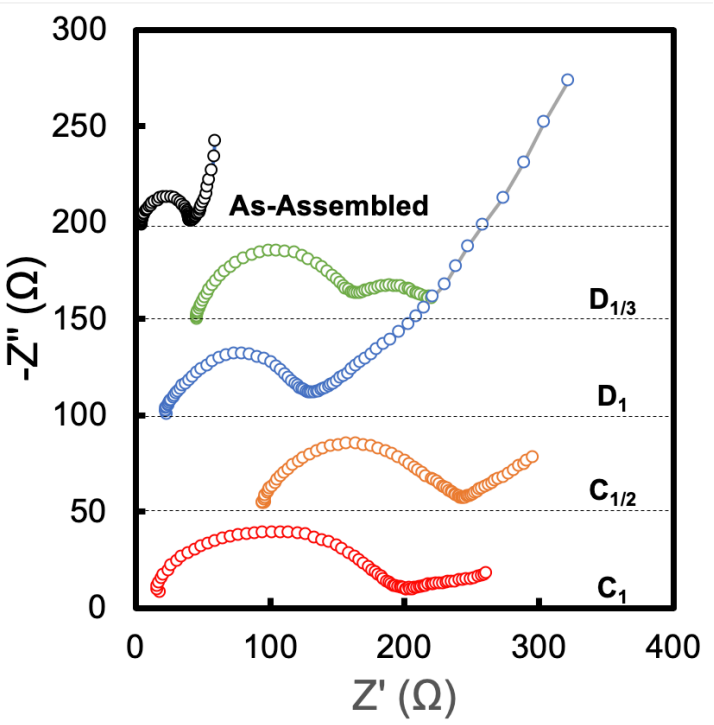

Figure S9. Post-mortem Nyquist plots from EIS measurements of various identical Li-Se batteries with originally hG/Se/hG sandwich cathodes (m_{Se} = 17.3 mg/cm^2, Se% ~ 75 wt%) that were discharged or charged to different extents at 1 mA/cm^2. The Nyquist plot from an as-assembled cell (the same shown in Figure 2a) is also shown for comparison.

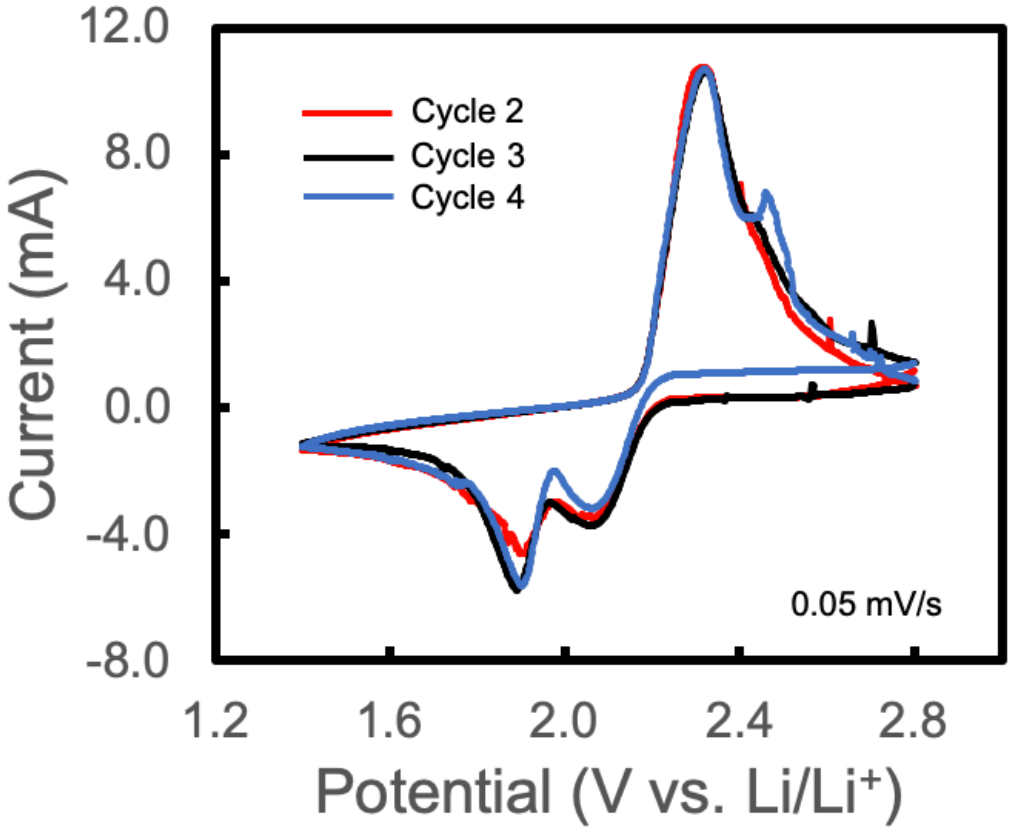

Figure S10. Cycles 2 – 4 of the CV measurements for a Li-Se battery with hG/Se/hG sandwich cathode (m_{Se} = 17.3 mg/cm^2, Se% ~ 75 wt%) at a scan rate of 0.05 mV/s with voltage limits of 1.4 (cathodic) and 2.8 V (anodic), respectively. These cycles were following Cycle 1 shown in Figure 2b.

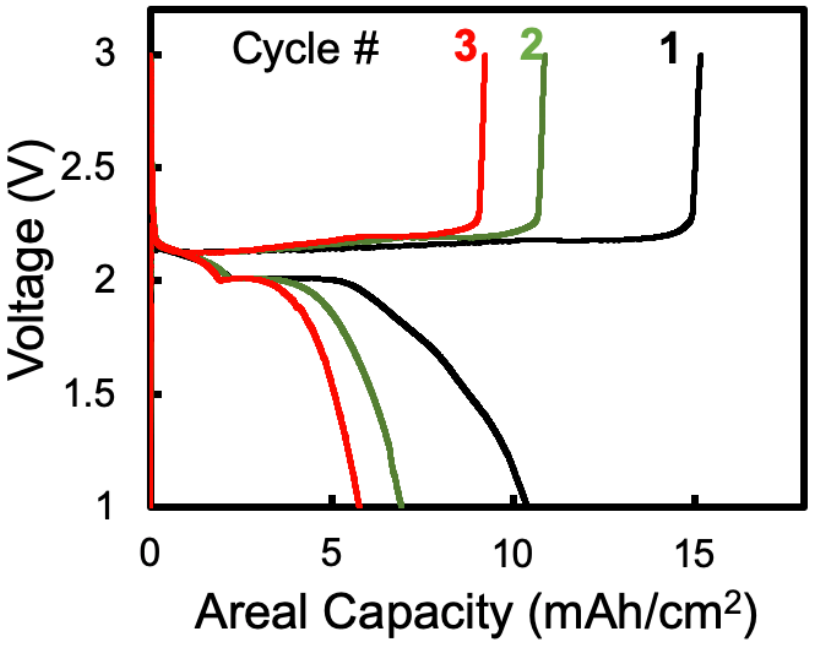

Figure S11. The first 3 cycles of a Li-Se battery with hG/Se/hG cathode (m_{Se} = 17.3 mg/cm^2, Se% ~ 75 wt%) at a current density of 0.5 mA/cm^2. The cycle 1 data is identical to that shown in Figure 2c.

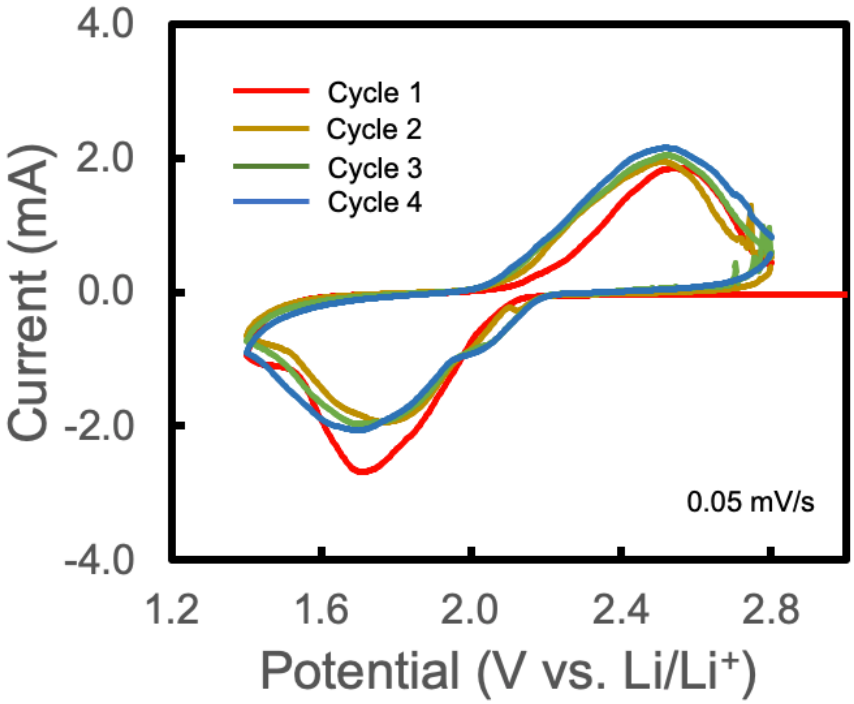

Figure S12. The first 4 cycles of the CV measurement for a Li-Se battery with hG/Se/hG sandwich cathode (m_{Se} = 17.3 mg/cm^2, Se% ~ 75 wt%) and TTE/DOL (1:1, v/v) as the electrolyte solvent. The scan rate was 0.05 mV/s; voltage limits were 1.4 (cathodic) and 2.8 V (anodic), respectively.

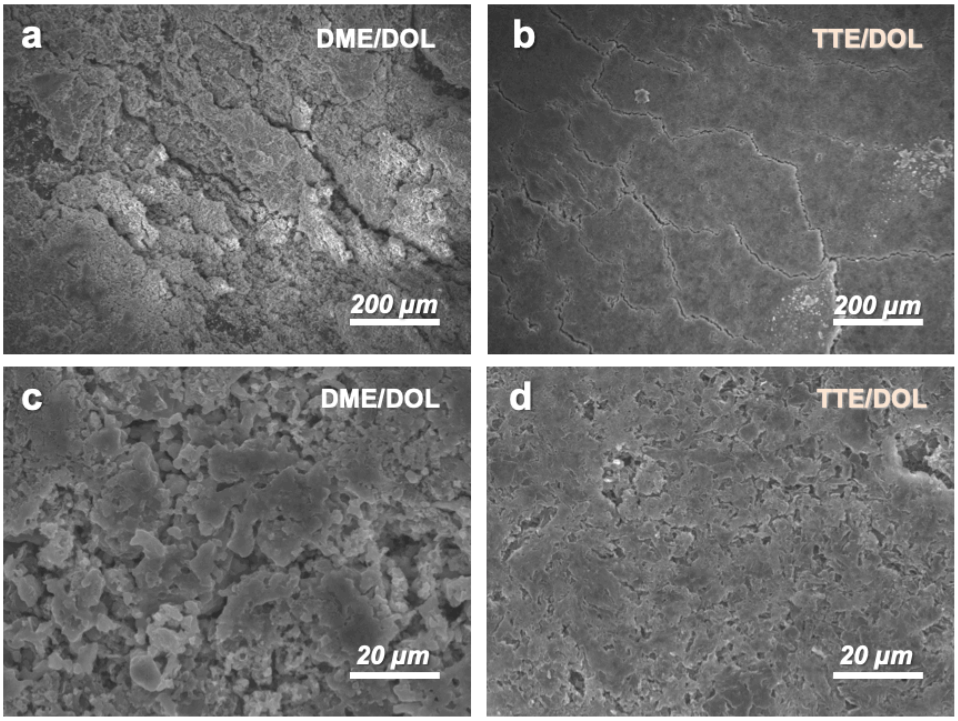

Figure S13. SEM images at (a,b) lower and (c,d) higher magnifications of post-mortem Li anode surfaces of Li-Se batteries with hG/Se/hG sandwich electrodes (m_{Se} = 17.3 mg/cm^2, Se% ~ 75 wt%) after prolonged cycling (> 80 cycles). The electrolyte solvents were (a,c) DME/DOL (1:1, v/v) and (b,d) TTE/DOL (1:1, v/v), respectively.

Table S1. Overall and layer density values (g/cm^3) of the sandwich discs measured via SEM. Density values of the neat active materials provided by the vendor (Sigma-Aldrich) are also listed for comparison.

	hG/Se/hG	hG/S/hG	hG/SeS_2/hG
Overall	2.31	1.46	2.09
hG Layer	1.09	0.81	0.97
Active Material Layer	3.68	2	3.41
Neat Active Material	4.81	2.07	N/A

Table S2. A literature survey (ordered roughly by date of publication) of available capacity values of various Se composite cathodes with Se mass loadings of > 3 mg/cm^2 in comparison to those in this work. Blue-shaded entries are those with high Se mass loadings of > 10 mg/cm^2.

Cathode Scaffold	Se Incorporation Method	Se Cathode Preparation	Se Content (%)	Se Mass Loading (mg/cm^2)	Current Density (mA/cm2) or [C-Rate]	Specific Capacity (mAh/g_{Se})	Areal Capacity (mAh/cm^2)	Electrolyte Base	Ref.
Holey Graphene	**Physical Sandwich with a Neat Layer**	**Dry Press**	**75**	**17.3**	**0.5/1/2/5**	**598.4/316.2/289.1/221.3**	**10.35/5.47/5.0/3.83**	**Ether (DME/DOL)**	**This Work**
					0.5/1/2/5	**466.7/288.6/154.3/38.10/**	**8.07/4.99/2.67/0.66**	**Fluorinated Ether (TTE/DOL)**	
3DPSe	Melt-Diffusion	3D Printed	48.2	4	0.5/1/2/ 3/5/8/10	657.7/568.3/ 531/512.4/ 485.1/441.6/401.9	2.63/2.27/2.12/2.05/1.94/1.77/1.61	Gel-Polymer	[S1]
				20		580/540/500/470/420/330/270	11.6/10.8/10/9.4/8.7/6.6/5.4		
Covalent Organic Framework	High-Speed Dispersion	Slurry Casting	80	~ 3	[6C/20C]	126/51	0.37/0.153	Ether (DME/DOL)	[S2]
Multilayer CNF	Syringe-Filtration	Syringe-Filtration	63.5	4.5/6.75	0.22/0.34	795/818	3.6/5.5	Ether (DME/DOL)	[S3]
				9.0/13.5	0.45/0.675	722/667	6.5/9.0		
ARC–SiOC	Melt-Diffusion	Slurry Casting	51.2	4/6	[0.1C]	850/616.6	3.4/3.7	Carbonate	[S4]
				8/10		600/350	4.8/3.5		
A4-Carbon Microspheres	Melt-Diffusion	Slurry Casting	60	3.2	1.6	513	1.64	Carbonate	[S5]
N,S Co-Doped Graphene Membrane	Solution Mix	Catholyte	N/A	~5	[0.5C/1C/ 2C/4C]	534.6/473.5/348.6/301.4	2.673/2.367/1.743/1.507	Li_2Se_8 Solution	[S6]
Dual-Doped Hierarchical Porous Carbon Matrix	Melt-Diffusion	Slurry Casting	~ 48	3	N/A	280	0.84	Carbonate	[S7]
PANI Coated Carbon Black	Melt-Diffusion	Slurry Casting	51.9	2-3	3.4/5.06/ 8.4 [2C/3C/5C]	529.2/514.2/475.6	1.3/1.29/1.19	Carbonate	[S8]
Nano-Cellulose Derived Monolithic Carbon	melt-Infiltration	Slurry Casting	70	6.64	[0.1C]	620	4.12	Carbonate	[S9]
CNTs	Pressure-Induced Melt-Diffusion	Slurry Casting	85	5–10	0.2C/0.5C/ 1C/2C	333/231/153/100	2.5/1.73/1.15/0.75	Ether (DME/DOL)	[S10]
G–SeHMs	Graphene Oxide /Se suspension	Slurry Casting	80	2–3	0.17/8.43 [0.1C/5C]	514/241	1.285/0.6	Ether (TEGDME/ DOL)	[S11]
Macro-/Micro-Porous Biochar-Based Framework	Melt-Diffusion	Slurry Casting	56.1	2.9±0.2	[0.2C]	466.8	1.35	Carbonate	[S12]

Multi-Walled Carbon Nanotube	Solution Mix	Slurry Casting	60.83	3.6	1.21/2.43 /4.86/9.72	~680/580/500/358.2	2.45/2.09/1.8/1.29	Ether (DME/DOL)	[S13]
Se	--	Slurry Casting	70	4	2.7 [0.5C]	546	2.18	Ether (DME/DOL)	[S14]
Porous Hollow Carbon Bubbles	Melt-Diffusion	Slurry Casting	48	3-4	[0.1C/0.2C/ 0.5C/1C	600/525/465/425	2.1/1.84/1.63/1.49	Carbonate	[S15]

References:

[S1] Gao, X.; Yang, X.; Wang, S.; Sun, Q.; Zhao, C.; Li, X.; Liang, J.; Zheng, M.; Zhao, Y.; Wang, J.; Li, M.; Li, R.; Sham, T.-K.; Sun, X. A 3D-printed ultra-high Se loading cathode for high energy density quasi-solid-state Li–Se batteries. *J*. *Mater*. *Chem*. *A* **2020**, *8*, 278-286.

[S2] Si, L.; Wang, J.; Li, G.; Hong, X.; Wei, Q.; Yang, Y.; Zhang, M.; Cai, Y. High energy density lithium-selenium batteries enabled by a covalent organic framework-coated separator *Mater. Lett.* **2019**, *246*, 144-148.

[S3] Xia, Y.; Lu, C.; Fang, R.; Huang, H.; Gan, Y.; Liang, C.; Zhang, J.; He, X.; Zhang, W. Freestanding layer-structure selenium cathodes with ultrahigh Se loading for high areal capacity Li-Se batteries. *Electrochem*. *Commun*. **2019**, *99*, 16-21.

[S4] Fang, R.; Xia, Y.; Liang, C.; He, X.; Huang, H.; Gan, Y.; Zhang, J.; Tao, X.; Zhang, W. Supercritical CO_2-assisted synthesis of 3D porous SiOC/Se cathode for ultrahigh areal capacity and long cycle life Li–Se batteries**.** *J*. *Mater*. *Chem*. *A* **2018**, *6*, 24773-24782.

[S5] Park, G. D.; Kim, J. H.; Lee, J.-K.; Kang, Y. C. Carbon microspheres with well-developed micro- and mesopores as excellent selenium host materials for lithium–selenium batteries with superior performances. *J. Mater. Chem. A* **2018**, *6*, 21410-21418.

[S6] Gu, X.; Xin, L.; Li, Y.; Dong, F.; Fu, M.; Hou, Y. Highly reversible Li–Se batteries with ultra-lightweight N,S-codoped graphene blocking layer. *Nano-Micro Lett*. **2018**, *10*, 59.

[S7] Zhao, X.; Yin, L.; Zhang, T.; Zhang, M.; Fang, Z.; Wang, C.; Wei, Y.; Chen, G.; Zhang, D.; Sun, Z.; Li, F. Heteroatoms dual-doped hierarchical porous carbon-selenium composite for durable Li–Se and Na–Se batteries. *Nano Energy* **2018**, *49*, 137.

[S8] Wang, B.; Zhang, J.; Xia, Z.; Fan, M.; Lv, C.; Tian, G.; Li, X. Polyaniline-coated selenium/carbon composites encapsulated in graphene as efficient cathodes for Li-Se batteries*Nano Res.* **2018**, *11*, 2460-2469.

[S9] Ding, J.; Zhou, H.; Zhang, H.; Tong, L.; Mitlin, D. Selenium impregnated monolithic carbons as free-standing cathodes for high volumetric energy lithium and sodium metal batteries. *Adv*. *Energy Mater*. **2017**, *8*, 1701918.

[S10] Dutta, D.; Gope, S.; Negi, D. S.; Datta, R.; Sood, A. K.; Bhattacharyya, A. J. Pressure-induced capillary encapsulation protocol for ultrahigh loading of sulfur and selenium inside

carbon nanotubes: Application as high-performance cathode in Li–S/Se rechargeable batteries. *J. Phys. Chem. C* **2016**, *120*, 51,29011-29022.

[S11] Youn, H.-C.; Jeong, J. H.; Roh, K. C.; Kim, K.-B. Graphene–selenium hybrid microballs as cathode materials for high-performance lithium–selenium secondary battery applications. *Sci. Rep.* **2016**, *6*, 30865.

[S12] Zhang, H.; Yu, F.; Kang, W.; Shen, Q. Encapsulating selenium into macro-/micro-porous biochar-based framework for high-performance lithium-selenium batteries. *Carbon* **2015**, *95*, 354-363.

[S13] Wang, X.; Zhang, Z.; Qu, Y.; Wang, G.; Lai, Y.; Li, J. Solution-based synthesis of multi-walled carbon nanotube/selenium composites for high performance lithium–selenium battery. *J. Power Sources* **2015**, *287*, 247-252.

[S14] Fang, R.; Zhou, G.; Pei, S.; Li, F. Cheng, H.-M. Localized polyselenides in a graphene-coated polymer separator for high rate and ultralong life lithium–selenium batteries. *Chem. Commun.* **2015**, *51*, 3667-3670.

[S15] Zhang, J.; Fan, L.; Zhu, Y.; Xu, Y.; Liang, J.; Wei, D.; Qian, Y. Selenium/interconnected porous hollow carbon bubbles composites as the cathodes of Li–Se batteries with high performance. *Nanoscale* **2014**, *6*, 12952-12957.